ADVANCED FUNCTIONAL MATERIALS
www.afm-journal.de

Materials Views
www.MaterialsViews.com

ITO-Free and Flexible Organic Photovoltaic Device Based on High Transparent and Conductive Polyaniline/Carbon Nanotube Thin Films

*Rodrigo V. Salvatierra, Carlos E. Cava, Lucimara S. Roman, and Aldo J.G. Zarbin**

The synthesis and characterization of thin films of polyaniline/carbon nanotubes nanocomposites is reported, as well as their utilization as transparent electrodes in ITO-free organic photovoltaic devices. These films are generated by interfacial synthesis, which provides them with the unique ability to be deposited onto any substrate as transparent films, thus enabling the production of flexible solar cells using substrates like PET. Very high carbon nanotube loadings can be achieved using these films without significantly affecting their transparency (≈80–90% transmittance at 550 nm). Sheet resistances as low as 300 Ω/□ are obtained using secondary polyaniline doping in the presence of carbon nanotubes. These films present excellent mechanical stability, exhibiting no lack in performance after 100 bend cycles. Flexible and completely ITO-free organic photovoltaic devices are built using these films as transparent electrodes, and high efficiencies (up to 2.27%) are achieved.

1. Introduction

Transparent and conductive thin films represent an important class of materials and are employed in a variety of technological applications including solar energy harvesters and light-emitting devices. Doped tin oxide films, among which indium-doped tin oxide (ITO) is the most widely used and well known, have been explored for nearly four decades and present excellent conductivities (≈10^3 S cm^{-1}) and transparencies (≈90% at 550 nm).[1,2] The search for a substitute for ITO films is an active research area due to the scarcity of indium, which in time will increase the market value because pure materials will become harder to find. Many materials are currently under investigation including metallic silver nanowire films,[3] evaporated metallic grids,[4] conjugated polymers[5] and nanocarbon structures such as carbon nanotubes (CNTs) or, more recently, graphene. Combinations of these materials are also the subject of active research.[6] Many of these alternative materials are utilized in attempts to achieve characteristics near those of ITO in terms of conductivity and transparency, but several other factors must also be considered such as the roughness, substrate adhesion, porosity and work function values.[1,7]

Although these alternative materials for ITO replacement present specific issues, they also exhibit new properties that are not achievable with ITO. For example, future optoelectronic devices (e.g., electronic paper, touch screens) must be flexible and stretchable to improve the robustness and extend the functionality of the devices. ITO, which is a ceramic material, can fracture even at low strain levels (<4%) and requires high temperatures and high vacuum systems in the production process,[2] but carbon nanotubes and graphene films can be deposited over flexible and transparent substrates such as PET under very mild conditions.

In addition to carbon nanostructures, some conducting polymers as PEDOT:PSS (poly(3,4-ethylenedioxythiophene:poly(styrenesulfonate)) and polyaniline (PANI) have been deeply investigated as ITO substitutes because of their conductivity, transparency and high work function values (>5 eV).[8] The conductivity value of these materials is strongly dependent on the chemical doping process. Doping in a conducting polymer is a complex process that includes the generation of charged species along the polymer backbone (solitons, polarons and bipolarons), as well as conformational changes in the polymer chains. This process results in highly delocalized charge carriers and thus produces the maximum conductivity that has been achieved in this class of materials.[9] Therefore, achieving high conductivity requires chemical control of the synthesis and properly choice of the so-called the primary (acids, oxidizing agents) and secondary dopants (solvents).[10–12]

By optimizing the transparency and the conductivity of thin films of PEDOT:PSS, high-efficiency, completely ITO-free light-emitting devices and solar cells have been constructed.[7,13] Applications of PANI, however, have generally been limited by its poor solubility (which makes difficult its processability as thin films). However, both the polymers PANI and PEDOT:PSS have been compared in several published papers as active materials for hole injection layers in solar cells, and more efficient devices

R. V. Salvatierra, Prof. A. J. G. Zarbin
Departamento de Química
Universidade Federal do Paraná (UFPR)
CP 19081, CEP 81531-990, Curitiba-PR, Brazil
E-mail: aldozarbin@ufpr.br
Dr. C. E. Cava, Prof. L. S. Roman
Departamento de Fisica
Universidade Federal do Paraná (UFPR)
CP 19081, CEP 81531-990, Curitiba-PR, Brazil

DOI: 10.1002/adfm.201201878

have been constructed using PANI films than PEDOT:PSS, due to the better work function and chemical resistance of PANI.[8,14,15]

Concerning the practical and widespread use of these conducting polymers in optical devices and transparent electrodes, one of the major challenge is related to the environmental stability, i.e., the ability to maintain electrical properties in the presence of long-term exposure to UV radiation and temperature fluctuations.[1,16] Producing nanocomposites of conjugated polymers through the incorporation of carbon nanomaterials (e.g., CNTs and graphene) is a very interesting solution, because these carbon nanomaterials exhibit improved conductivity (by several orders of magnitude) and enhanced chemical and thermal stability.[17] These properties lead to devices with better performance, as previously reported in devices such as solar cells.[18,19] Moreover, the preparation of CNTs/conducting polymer nanocomposites can also solve another problem related to the utilization of CNTs and graphene thin films for ITO replacement: the research into thin films of these nanomaterials seems to be limited by their high sheet resistances and low transparencies, which are ultimately related to the sample purity, assembly of the film, wettability, tube length, and the method of film production. The bulk conductivities of these CNT films can vary drastically (10–6000 S cm^{-1}), as the bulk conductivity does not reflect the conductivities of the individual components (≈200 000 S cm^{-1}).[1] This variation has been demonstrated to be related to the high junction resistance (ca. 1000 Ω) between each individual nanotube. To overcome this limitation, oxidative treatments and lengthy, expensive purification procedures have been performed to improve the tube-tube contact and thus obtain films with very low resistances.[20] Ma and coworkers presented an approach to minimize the contact resistance by incorporating a thin layer of polyaniline derivative that acts as conductive glue between tubes, resulting in a CNT-based sample that exhibited increased conductivity and a reduced percolation threshold.[21]

Recently, we reported a suitable and simple interfacial polymerization method for the synthesis of polyaniline/carbon nanotube nanocomposites that were obtained directly as transparent, homogeneous, and conductive thin films.[22] This synthetic route, that was further extended to graphene-based nanocomposites and neat carbon nanotubes films,[23,24] produces high-quality films with a really good conductivity. However, the transparence (50–60%) was not adequate for the utilization as transparent electrode. In this work, we present a huge improvement on the quality, conductivity and transparence of these CNTs/polyaniline nanocomposites thin films by: 1) decreasing the diameter of the CNTs employed to prepare these materials, and 2) submitting the PANI:CNT film to a secondary doping process. The optimized film was subsequently used as a transparent conductor (anode) in a flexible and ITO-free organic photovoltaic (OPV) device, showing outstanding performances, superior to those of similar devices built with ITO as anode. This is the first report on an OPV device using this kind of nanocomposite as a transparent electrode.

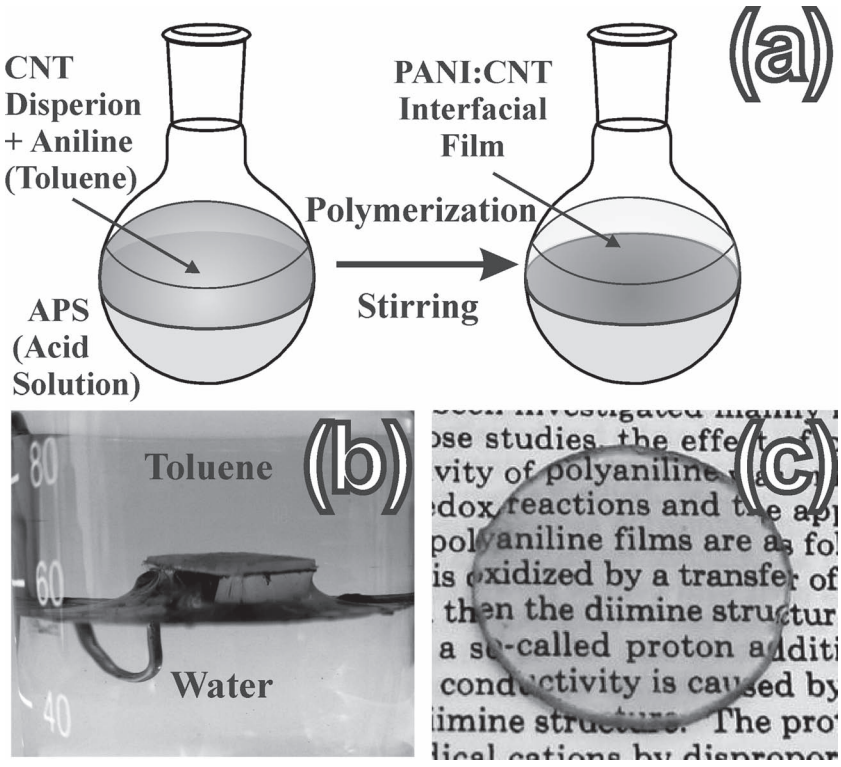

Figure 1. a) Scheme of interfacial polymerization in the presence of a carbon nanotube dispersion; b) glass support being lifted and removing an interfacial film; c) nanocomposite film (PANI:CNT) over glass substrate. The original color of the film in (b) and (c) is pale green.

2. Results and Discussion

2.1. Self-Assembled Thin Films of Carbon Nanotubes and Polyaniline

Self-assembled films of polyaniline and multiwalled carbon nanotubes were produced by interfacial polymerization as described in our previous paper.[22] This synthesis technique allows the carbon nanotubes to assemble at the liquid-liquid interface and then participate in the polymerization reaction, in which the monomer (aniline) and oxidant (ammonium persulfate–APS) are separated into organic (oil) and aqueous phases, respectively, as schematically shown in **Figure 1**a. As a hybrid material, the interfacial film is highly flexible and elastic. Figure 1b presents a picture of a glass substrate being lifted and stretching the thin interfacial film (<100 nm). The stabilization of particles at the liquid-liquid interfaces (oil/water interfaces) and the astonishing mechanical resistance of such thin films result from minimizing the free energy of the system in the presence of the many interaction forces between the particles and the two liquids; in this case, the free energy is represented by the interfacial tension between toluene and water (36 mN m^{-1}). The particles themselves in both solvents can also interact through van der Waals, steric, and electrostatic

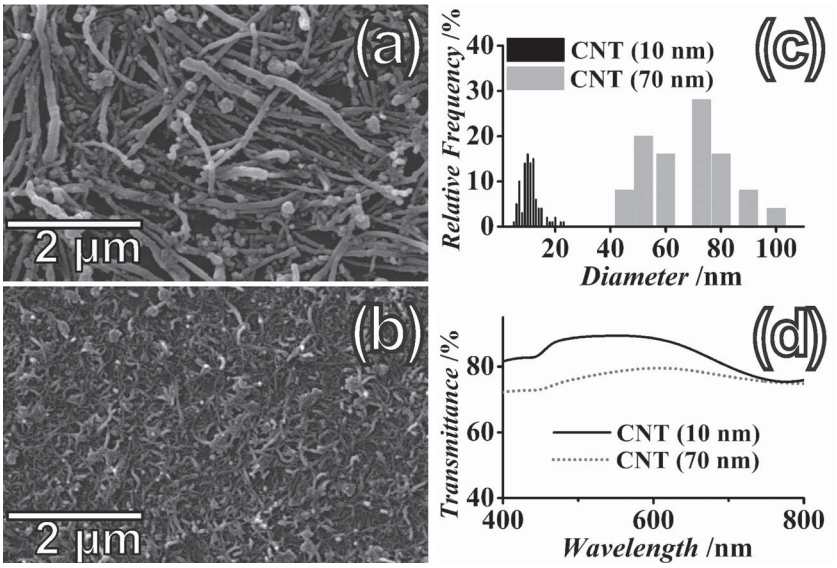

Figure 2. a) SEM images of PANI:CNT nanocomposite starting from CNTs of 70 nm diameter; and b) SEM images of PANI:CNT nanocomposite starting from CNTs of 10 nm diameter; c) histograms showing the diameter distribution of the two CNTs samples; d) transmittance spectra of PANI:CNT films prepared from the two different CNT samples.

forces, which can lead to highly ordered interfacial organization.[25,26] Similar films can also be produced at the water-air interface (after toluene evaporation) at which an even higher interfacial energy exists (75 mN m^{-1}). However, films produced at this way (water/air interface) exhibit reduced flexibility and elasticity, evidencing the important role of the liquid nature of the interface. By spreading this tri-phasic system (water/film/oil) over suitable substrates (quartz, PET, silicon, etc.), highly homogeneous and transparent films of insoluble materials can be obtained, as can be seen in Figure 1c.

To fully utilize the properties of these hybrid thin films, the carbon nanotube material must be chosen to optimize the conductivity and transparency and to prevent the creation of an inhomogeneous surface. **Figure 2**a,b present scanning electron microscopy (SEM) images of two hybrid thin films obtained using the same amount of multiwalled carbon nanotubes with different diameters (average values of 70 and 10 nm, respectively, as can be seen in the histogram present in Figure 2c). The average lengths of these carbon nanotubes are close to 2 and 1.5 μm. The film produced using the larger diameter nanotubes (Figure 2a) is thicker (≈190 nm) and exhibits a very inhomogeneous topography (noncovered regions of the glass substrate are clearly seen in the Figure 2a). The film produced using the smaller diameter nanotubes (Figure 2b) is thinner (≈50 nm) and covers the entire substrate. The dispersion in the diameter distribution of the larger nanotubes is also three times higher than that of the thinner nanotubes, as shown in Figure 2c.[27] This discrepancy may lead to poorer assembly of carbon nanotubes at the liquid interface and thereby contribute to a nonuniform film. Thus, small-diameter nanotubes and/or low diameter dispersion are crucial to the production of high-quality films. Another critical factor is the effect of the carbon nanotube size on the transparency of the films. As presented in the transmittance spectra in Figure 2d, the larger multiwalled carbon nanotubes, which are composed of a higher number of concentric graphene sheets, lead to darker films. Next, we describe the characterization of the carbon nanotubes/polyaniline films produced using the thinner carbon nanotubes.

Figure 3 presents a photograph of four different polyaniline films with different carbon

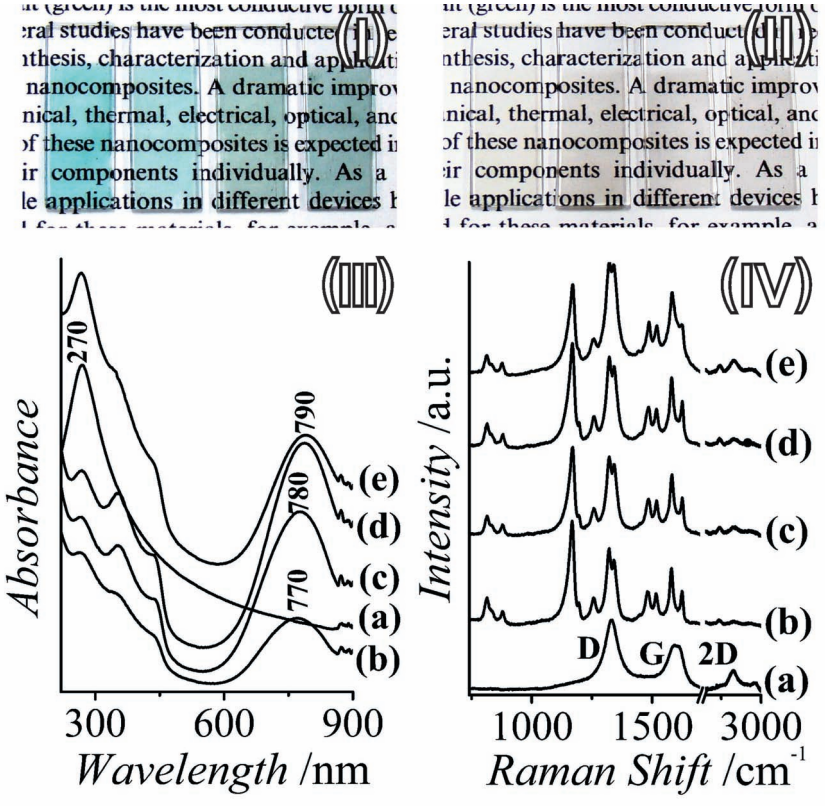

Figure 3. Digital photographs of the four interfacial films, deposited over glass substartes, before (I) and after (II) the secondary doping of polyaniline. From left to right: PANI:CNT2, PANI:CNT5, PANI:CNT7, and PANI:CNT10; III) UV-vis and IV) Raman spectra of the four different interfacial films: a) CNT5, b) PANI:CNT2, c) PANI:CNT5, d) PANI:CNT7, and e) PANI:CNT10.

nanotube loadings (see the Experimental Section), before (Figure 3I) and after (Figure 3II) the secondary dopping (as will be discussed further). A film containing only CNTs at 5.0 μg mL^{-1} concentration (CNT5) was also produced for comparison. The CNT content is determined by adding the same volume of dispersions of different CNT concentrations into the same amount of aniline monomer at the same oxidant ratio (see the Experimental Section). An important factor that should be mentioned is that neat polyaniline (at the same concentration) could not be synthesized without the presence of the carbon nanotubes, even after four days of reaction. As previously observed by us and other authors, the CNTs act as seeds for polymer growth (heterogeneous nucleation), and their presence can be critical under specific conditions, primarily under diluted conditions as utilized in interfacial polymerization.[22,28]

The presence of carbon nanotubes in these green films (typically of an emeraldine salt color) is demonstrated by absorption and Raman spectroscopy, presented in Figure 3III,IV, respectively.[29] The Raman spectra of all films show, besides the typical carbon nanotubes bands (D, G, and 2D), all the bands associated to the polyaniline, emeraldine salt, confirming the occurrence of this polymer in all samples.[29] The absorption spectra of the films (Figure 3III) contains the three primary electronic transitions of polyaniline-emeraldine salt at approximately 350, 440, and ≈780 nm.[9,30] The first band is due the band gap of the polymer (≈3.2 eV), and the other two bands are assigned to polaronic/bipolaronic transitions created inside the gap by the acidic doping. The band at ≈780 nm is indeed attributed to a mixed state of localized polarons and bipolarons whose population is regulated by several factors such as organization, chain conformation and doping level.[31] This band is increasingly red-shifted as the CNT content increases (from 770 to 780, 790, and 790 nm in the films PANI:CNT2, PANI:CNT5, PANI:CNT7, and PANI:CNT10, respectively), thus confirming the presence of more extended chains where close contact between the polymer and CNT sidewalls exists. The CNT transition at approximately 270 nm (Figure 3III) is also visible in each spectrum. The intensity of this band is determined by the amount of CNT in the interfacial film. The 270 nm band is associated to a localized π–π^* transition and is present in the electronic spectra of all sp^2 carbon species including single-walled and multiwalled carbon nanotubes and graphene.[32] The spectra demonstrate that the absorbance increases as the CNT content in the films is increased. However, a pure CNT interfacial film (CNT5) has a higher absorbance than the corresponding films containing polyaniline (PANI:CNT5), at least at wavelengths below 600 nm. This observation can be attributed to the expansion of the CNT network as the films are filled with the polymer, which grows around the CNT sidewalls.

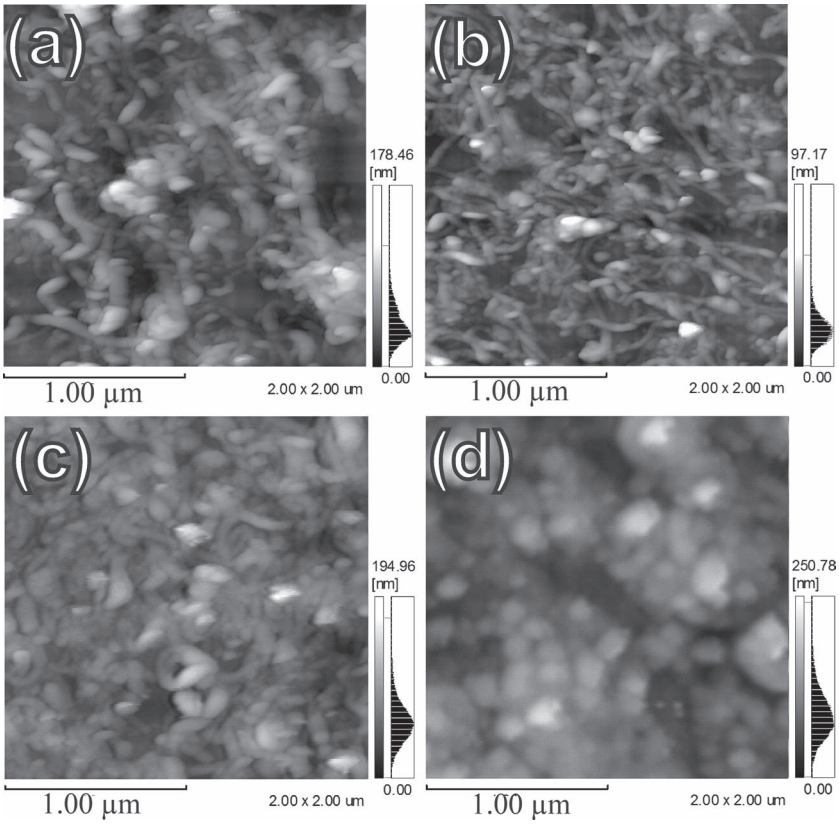

Figure 4. Topographic AFM images of the films a) PANI:CNT2, b) PANI:CNT5, c) PANI:CNT7, and d) PANI:CNT10.

Figure S1 (Supporting Information) shows the SEM images of the PANI:CNT films. The image of CNT5 is also presented in Figure S2. The images show that the films are flat carpets with tubular structures lying in the plain of the film. As expected, the amount of CNT in the films increases as their concentration of the dispersion increases. Isolated portions of polymer or CNT structures are not observed anywhere within the films, except in the case of the sample containing the highest concentration of CNT (sample PANI:CNT10), in which isolated bundles of CNTs have been observed.

Figure 4 present the atomic force microscopy (AFM) images of the films. These images show very compact films in which tubular structures connected to each other along the surface. A few bright points are observed in the images and correspond to points of increased height. These structures could be polymer chains or CNTs that are vertically oriented. Despite the rough nature of the surface, the morphology is very regular, which will be shown to be very important to the study of these films as conducting layers in OPV devices. The roughness of these materials naturally arises from the hybrid nature of the films and the fibrous growth of the polymer; thus, the roughness of the films will depend on the CNT concentration and on the grown mechanism of the polymer. Figure S3a (Supporting Information) presents the dependence of the thickness and root mean square (RMS) roughness of the films (obtained by AFM) in function of the CNT concentration. The change in thickness is proportional to the amount of CNT in the film, whereas

the roughness is not equally proportional. Rougher surfaces (≈30 nm) are observed at the extremes (highest and lowest CNT concentrations, (PANI:CNT10 and PANI:CNT2). In the first case, the roughness is associated to the bundled structures as discussed before, whereas in the latter case, the polymerization is less CNT-assisted (excess of polymer), and region containing only polyaniline nanofibers (without the presence of CNTs) may be formed. The PANI:CNT5 film is the least rough film (12 nm), and this value reflects the nature of the film observed in SEM and AFM measurements.

The effects of CNTs on the transmittance at 550 nm and the conductivity are presented in Figure S3b (Supporting Information). As expected, the transmittance is decreased as the CNT concentration of the film increases. However, increasing the CNT concentration does not seem to directly increase the overall bulk conductivity of the material. The highest conductivity of 22.1 S cm^{-1} is found for the PANI:CNT5 film, which also exhibits a transmittance of 89.4% at 550 nm. The sheet resistance of this film is 85 kΩ/□. The most conductive film is also the least rough, with an average roughness of 12 nm. The reason for the low conductivities of the high CNT-concentration films is related to the interference between the CNTs in the polymer formation process. Although CNTs can act as seeds for the initial polymer growth, their influence in the polymerization reaction should not be neglected. The ammonium persulfate (APS) used to oxidize the anilinium anion can also react with CNTs. This effect is weak at low CNT concentrations, but at higher concentrations (PANI:CNT7 and PANI:CNT10), the presence of the CNTs can alter the aniline:APS molar ratio (see the Experimental Section), also known as the K parameter. This ratio is critical in the polymer formation process and can dramatically affect the yield and, most importantly, the conductivity.[33] This effect can be observed only in diluted reaction regimes like that employed in interfacial polymerization. Subsequent studies should investigate a correction to the oxidant concentration proportional to the amount of added carbon (carbon nanotubes or graphene). Thus far, we have seen that very compact films can be formed and that the CNT concentration clearly influences the film properties. However, in applications, high transparency and surface regularity must be combined with high conductivity; thus, we proceed with secondary doping in the polyaniline aiming to increase the conductivity of these films.

2.2. Highly Conductive PANI:CNT Films Over Flexible Substrates

The secondary doping of polyaniline is a well-known process that changes the chain conformation of polyaniline from a compact coiled form to a more expanded form through the proper choice of acids (primary dopant) and solvents (secondary dopant).[34] The most well-studied system is polyaniline doped with camphorsulfonic acid (CSA) and casted from or exposed to meta-cresol solvent. The expansion of the chains creates a more conjugated system and thus a more conductive polyaniline that can achieve metallic behavior.[35] Thus, we performed the synthesis of PANI:CNT films with polyaniline doped with CSA, and exposed them to meta-cresol vapors (see the Experimental Section). **Figure 5**I presents the absorption spectra of all PANI/CSA:CNT films before and after exposure to meta-cresol vapors. When we de-doped the PANI:CNT films and redope with camphorsulfonic acid (before the secondary doping), the same films show less pronounced red-shifts, when compared to the sulfuric acid doped samples (spectra presented in Figure 3III). We believe that the de-doping process lead to the shrinkage of PANI chains, even in the presence of relatively rigid CNT, and further doping with a large organic acid (CSA) do not recover the extended chains of PANI, which is observed only after the secondary doping. In all spectra of the secondary doped samples (Figure 5I) we observe a large red-shift in the localized polaronic transition band, as well as a decrease in its intensity due to the secondary doping. As a result, the films lose their green color (as showed earlier in the picture of Figure 3II). This red-shift is also observed in CSA-doped polyaniline exposed to meta-cresol vapors and is accompanied by an increase in the intensity of the

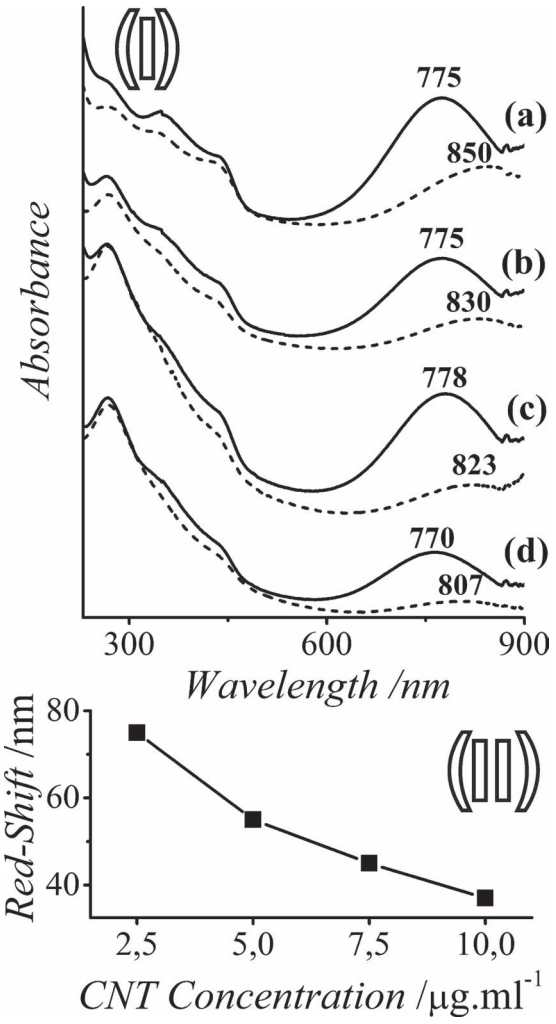

Figure 5. I) UV-vis absorption spectra of PANI:CNT films at different concentrations before (full lines) and after (dashed lines) exposure to meta-cresol vapors: a) PANI:CNT2, b) PANI:CNT5, c) PANI:CNT7, and d) PANI:CNT10; II) red shift of the localized polaron transition after the exposition to meta-cresol vapors as a function of the CNT content.

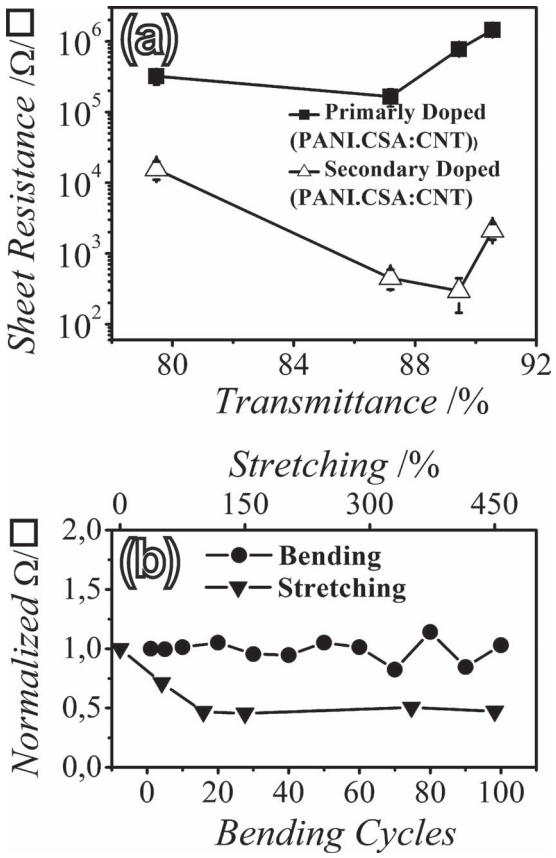

Figure 6. a) Sheet resistance vs transmittance at 550 nm for the four PANI:CNT films before (square) and after (open triangles) the meta-cresol exposure; b) the normalized sheet resistance of PANI:CNT5 film deposited over PET after 100 bending cycles (circles) and stretching (triangles).

free carrier transition in the near infrared (see Figure S5), indicating the creation of additional delocalized charge carriers due to the transition from the coil-like conformation to the expanded coil-like conformation. However, the red-shift decreases proportionally to the increases in the CNT content (as can be seen in Figure 5II), which suggests that the presence of CNTs produces films that are more chemically resistant to vapor exposure. This resistance arises because the CNTs create a physical barrier to polymer chain extension, and a similar effect has been observed with composites of structural polymers and CNTs.[36,37] The secondary doping has a huge effect on the conductivities of these PANI:CNT films, as can be observed in **Figure 6**a, that illustrate the dependence of the sheet resistance and of the transmittance at 550 nm of CSA-doped PANI:CNT films before and after the meta-cresol exposure. The sheet resistances of the PANI:CNT films change in a complex way due to multiple effects such as the chemical resistance to secondary doping induced by the presence of CNTs, the CNT conductivity and the characteristics of the polymer synthesized in the presence of CNTs. The presence of the CNTs in these films is critical to achieving such low resistances because the CNTs create a percolation network throughout the film even though they also create a barrier to the full extension of the polymer chain. An optimal sheet resistance of 295 Ω/□ with 89% transmittance at 550 nm is attained by the PANI:CNT5 film.

The interfacial film can also be deposited onto any substrate, including PET or rubber substrates, which make these films strong candidates for flexible, transparent electrodes. The conductivity of the film PANI:CNT5 deposited over PET are kept constant after a cycle of 100 bending these films (30 degrees), as observed in Figure 6b. This property is not possible for metal oxide (ITO)-based electrodes, as these materials are brittle.[1] We also show that the PET/PANI:CNT5 electrode can be stretched to at least 50% of their original dimensions without loss of conductivity (Figure 6b). Polyaniline is known to exhibit improved conductivity when stretched because of the longer conjugation paths resulting from chain alignment in the stretching direction.[38] The results showed here demonstrate clearly that we obtained transparent, flexible and stretchable electrodes. Electrodes presenting all these characteristics together are very hard to produce, and very few systems are currently under study for use in future flexible and stretchable devices.[39] Thus, the next step was verifying the viability of the application of this electrode in a real device. The transparent electrodes obtained by interfacial polymerization were then employed as ITO substitutes in organic photovoltaic devices.

2.3. Photovoltaic Devices Using PANI:CNT Electrodes

Transparent electrodes for organic photovoltaic cells needs very low sheet resistances combined with high transparencies, to prevent a high series resistance while allowing the photons to reach the active layer. In order to prepare the flexible OPCs, the PANI:CNT films were deposited over plastic (PET) substrates and used as transparent electrodes. **Figure 7** shows the scheme of the device building, using a bilayer architecture composed of F8T2 (poly[9,9′-dioctyl-fluorene-cobithiophene]) and C_{60}, as well as a picture of the device, showing its flexibility. For comparison, similar devices have been built using commercial ITO and FTO electrodes, as well as electrodes composed of neat-CNTs films (without polyaniline). The fluorene-thiophene polymer employed (F8T2) as active layer was chosen due to its good roughness, electronic energy that matches very well with both electrodes, and because its well-known high efficiency in bilayer architectures.[40]

The use of the PANI:CNT nanocomposite as transparent electrodes presents other experimental advantages that impact directly on the efficiency of the device. For example, there are some reports on the preparation of flexible photovoltaic devices constructed with PEDOT:PSS as electrodes, also deposited over PET substrates. This deposition normally requires surfactant-assisted dispersion (Zonyl) of the PEDOT:PSS, to achieve better wettability on the PET substrates, which results in a lower conversion efficiency due the contamination of the active layer by the surfactant.[39] In our devices the PEDOT:PSS films were easily and uniformly spin-coated over a PET/PANI:CNT electrode without the use of any additional surfactant, attributed to a better interaction between the PEDOT:PSS and the PET/PANI:CNT electrode. Contact angle measurements have shown that the PEDOT:PSS solution has a better wettability with the PANI:CNT electrode than with ITO (as can be seen in Figure S4,

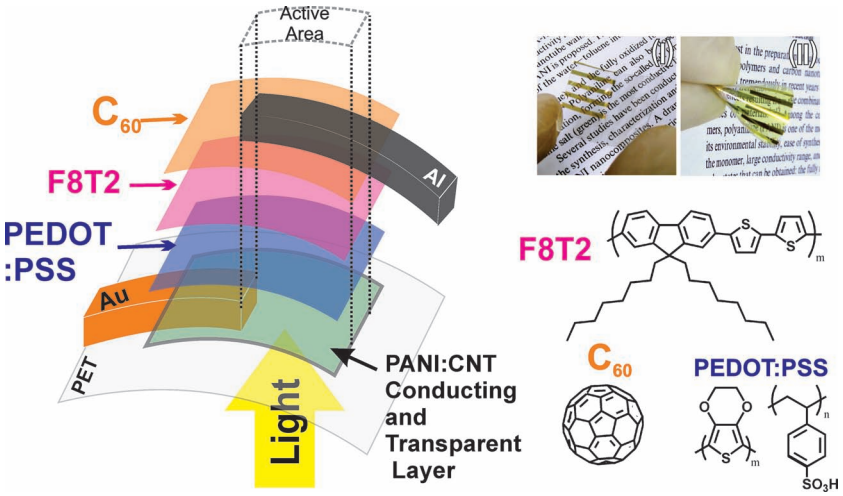

Figure 7. The configuration of the solar cell built over a PET/PANI:CNT5 film, and the corresponding chemical structures of the organic layers. The photographs show the PET/PANI:CNT:5 film (I) and the flexible solar cell (II).

Despite the great advantages of the PANI:CNT films, their properties do not seem to affect other device characteristics. The fill factors (FF),[41] which are ultimately related to the series resistance of the device (limited in these cases by the anode), are very similar for devices built using ITO, FTO, and PANI:CNT. The V_{OC} value of the PANI:CNT device is also very similar to that observed for ITO device. The V_{OC} is related to the energy difference between the HOMO (highest occupied molecular orbital) level of the donor polymer (F8T2) and the LUMO (lowest unoccupied molecular orbital) level of the acceptor (C_{60}) and to the work functions of the electrodes (PEDOT:PSS and Al). A lower value of V_{OC} (0.52 V) was observed for the neat CNT-based anode and could be related to its porous nature, which can affect the PEDOT:PSS layer to some extent. A highly conductive PEDOT can lead to a current leak, which reduces the V_{OC}, as described elsewhere.[42]

Supporting Information), which demonstrates a favorable interaction between the polymeric layers. Indeed, polyaniline has proven to be much more robust than PEDOT:PSS in several optoelectronic devices (OLED and OPVs), showing improved chemical resistances and resistance against ultraviolet radiation.[8] In our electrodes the presence of CNTs also provides a beneficial contribution increasing the chemical resistance and the stability against radiation.

Figure 8a shows the transmittance spectra of the PANI:CNT5, ITO, FTO (fluorine-doped tin oxide) and CNT films-based electrodes, as well as the spectrum of neat F8T2 (spin-coated film). Figure 8b shows the current density (J) versus the applied bias (V) curves for photovoltaic devices built over the flexible transparent electrodes based on PANI:CNT5 and neat CNT films, as well as for similar devices built over commercial glass electrodes covered with with ITO (≈10–20 Ω/□, T% = 97% at 550 nm) and FTO (≈5–20 Ω/□, T% = 80% at 550 nm). **Table 1** shows some experimental data collected from these devices. Strikingly, the highest short-circuit currents (J_{SC}) were obtained for the PANI:CNT- and CNT-based devices (6.85 and 4.87 mA cm^{-2}, respectively), whereas the highest power-current efficiency (PCE) was achieved by the device prepared from the PANI:CNT film (2.27%). The reason for such high short-circuit currents is believed to be related to a higher active area for exciton generation in ITO-free cells because these devices have a rough (but regular) surface instead of the relatively flat surfaces of ITO and FTO. This effect is evidenced by the values of J_{SC}. The similar behavior (J–V characteristics) observed for these two metal oxide films (ITO and FTO) emphasizes the distinct features of the PANI:CNT film. Due the rough surface of the CNTs covered with PANI, both the PEDOT:PSS and the active layer (F8T2) also became rough, matching the surface morphology of the PANI:CNTs. The same effect must occur with the neat CNT film, but in this device the transmittance is lower and the sheet resistance is higher. Therefore, the fill factor is the lowest among all the studied device. These results were highly reproducible in several similar devices studied.

It is often observed that ITO-free devices based on polymers (like PEDOT:PSS) or carbon nanomaterials (CNT, graphene)

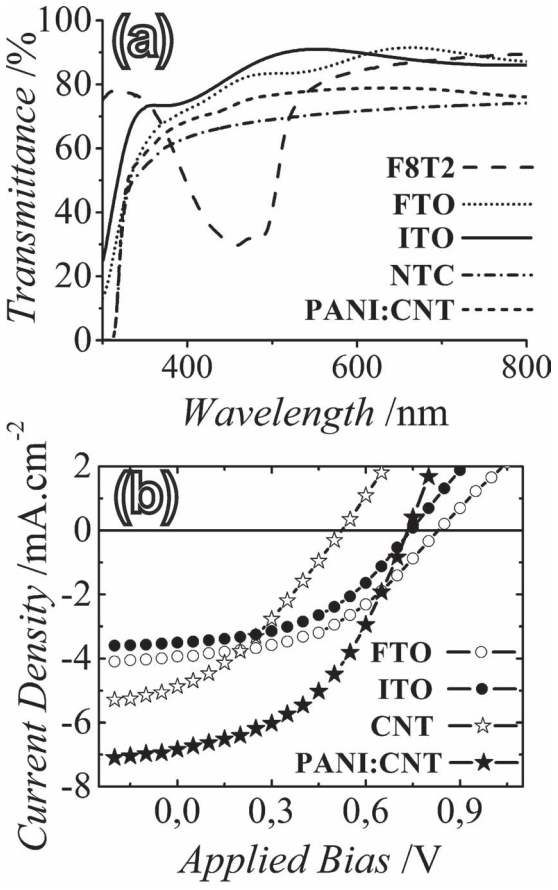

Figure 8. a) Transmittance spectra of different films (glass/ITO, glass/FTO, PET/CNT and PET/PANI:CNT); b) current density (mA cm^{-2}) vs voltage (V) for the different anodes used in the solar cells.

Table 1. Experimental data extracted from the photovoltaic cells built with different materials as the transparent anode (cell architecture: anode/PEDOT:PSS/F8T2/C_{60}/Al).

Anode	V_{OC} [V]	J_{SC} [mA cm^{-2}]	FF [%]	PCE [%]
Glass/ITO	0.74	3.51	45.9	1.20
Glass/FTO	0.83	3.95	44.8	1.47
PET/CNT	0.52	4.87	32.8	0.83
PET/PANI:CNT	0.73	6.85	45.1	2.27

show relatively lower efficiency than the ITO-based similar cells.[1,20] Nevertheless, our device presents one of the highest efficiency values (2.27%) found in the literature until now for ITO-free flexible solar cells. A non-exhaustive search in the literature shows the best value of 2.8% efficiency for the solar cell presented by Rowell and co-workers using modified PEDOT:PSS films.[7,43–45] Our results become exciting if we bear in mind that a very simple synthetic procedure is employed to obtain the interfacial films, as well as to build the solar cell (all the manipulation was carried out at ambient conditions). With respect to ITO-free and nonflexible solar cells (constructed over rigid substrates like glass or quartz), it is possible to find even higher values, for example, 4.13% for a cell based on a single-wall CNT film.[46] All the efficiency values found in literature must be carefully compared, as the solar cells are constructed in very different ways and several aspects must be taken into account, like thermal annealing, exposure to atmosphere, moisture, and the presence of buffer layers. Moreover, it is important to note that most ITO-free devices report the use of bulk heterojunction solar cells with P3HT:PCBM (poly(3-hexylthiophene):[6,6]-phenyl-C_{61}-butyric acid methylester) since it is a well-known system and generally presents better efficiencies values than the bilayer counterpart.[43,47] In this context, the ITO-free bilayer solar cell presented in this work shows a high efficiency in a unusual configuration. Finally, the polymer F8T2 was never presented before as the active layer in an ITO-free cell. This polymer has a peculiar liquid crystalline phase property, thus contributing to a better efficiency in this bilayer configuration.[48]

Finally, this work demonstrates the possibility of preparing similar devices without the PEDOT:PSS layer. As the PANI and PEDOT have similar work functions, in theory, the PANI could act as both the transparent conductor and the hole transport layer. Research in this direction is currently underway in our laboratory.

3. Conclusions

We prepared highly conductive and transparent polyaniline/carbon nanotube interfacial thin films, exhibiting a transmittance of 89% at 550 nm and a sheet resistance of 295 Ω/□, by choosing the appropriate characteristics of the CNTs and optimizing the conductivity of the polyaniline through a secondary doping process. Besides the excellent transparency and conductivity, the presence of CNTs improves the chemical resistance of the films. In addition, these films can be easily deposited onto flexible and stretchable substrates, and have shown good mechanical stability and maintenance of conductivity and transparence after several cycles of bending and stretching. Organic photovoltaic cells were built using these interfacial films as transparent anodes in flexible ITO-free devices, resulting in better efficiencies when compared to ITO-based equivalent devices. The superior performance has been attributed to the better interactions of the anode to the PEDOT:PSS layer, as well as due to the higher short-circuit current (J_{SC}) produced by the rough but regular surface of the PANI:CNT films (which increases the active area of the device). The results indicate that novel ITO-free optoelectronic devices can be optimized with very high performance using interfacial films of conjugated polymers and carbon nanomaterial species.

4. Experimental Section

Materials: Toluene (Carlo Erba), DMSO (dimethylsulfoxide–Carlo Erba), H_2SO_4 (sulfuric acid–Carlo Erba), C_{60} (fullerene–SES Research), poly(9,9′-dioctylfluorene-alt-bithiopehene) (F8T2, M_n > 20 000 g mol^{-1}; Aldrich), (+)camphorsulfonic acid (HCSA, Merck), APS (ammonium persulfate) were used as received. Aniline and meta-cresol were bi-distilled before use. CNTs of 70 nm diameter (average length: 2 μm) were synthesized through a CVD method using ferrocene ($C_{10}H_{18}Fe$) as the metal precursor and carbon source, as previously described.[49] CNTs of 9.5 nm diameter and an average length of 1.5 μm were purchased from Nanocyl. The relative frequency of CNTs were obtained through TEM measurements. The samples were purified as described elsewhere.[22] PEDOT:PSS solutions (CLEVIOUS Al 4083) were filtered through a syringe filter (0.45 μm pore size) before use.

Synthesis of PANI:CNT Interfacial Films: 20.0 mL carbon nanotube dispersions in toluene (Nanocyl) at concentrations of 2.5, 5.0, 7.5, and 10.0 μg mL^{-1} were used. The dispersions were produced in an ultrasonic bath (154 W, 37 Hz) for 1 h at 0 °C. A dispersion of 7.0 μg mL^{-1} of 70 nm CNTs were used for comparison. 1.0 mg of APS was dissolved in 20.0 mL of H_2SO_4 1.0 M inside of a 50 mL round bottom flask and magnetically stirred at 3000 rpm. Aniline (1.5 μL) was added to 20.0 mL of the toluene dispersion, and this dispersion was added to the aqueous phase. After 12 h, a green film was observed at the liquid-liquid interface. To remove oligomers, the organic and the aqueous phases were removed and fresh toluene and acid solution (sulfuric acid 2 M) were added. This process was repeated several times. The three-phase system (toluene/film/water) was transferred into a beaker in which the substrate (PET, quartz, or glass) was already placed. The substrates were then lifted in the direction of the film, and the substrate/film was dried in air. The different samples prepared in this work, as well as some experimental details, are given in **Table 2**.

Secondary Doping of PANI:CNT Thin Films: The first step was the preparation of nanocomposite films with the polyaniline deprotonated, in the so-called emeraldine base (EB). The synthesis of the nanocomposite films was carried out exactly as described before, but during the washing process, the replacement of the aqueous phase is carried out with a NH_4OH 1.0 M aqueous solution, followed by deionized water until the films are equilibrated with pH = 7. The characteristic blue color of the PANI emeraldine base was verified. The films were deposited in PET or quartz for absorption measurements and left to dry under a dessicator for 12 h. This step is necessary to obtain good adhesion of the film to the substrate. After 12 h, the films were dipped for 12 h in an aqueous solution of camphorsulfonic acid 0.1 M for reprotonation. A pale green color was achieved. The films were then dried under an argon flow and placed inside of a desiccator saturated by vapors of meta-cresol for five days to obtain the secondary doping.

Table 2. Experimental data for the preparation of the polyaniline:carbon nanotube interfacial films.

Film	Aniline [μL]	CNTs [μg mL^{-1}]	CNTs:Aniline ratio [w/w]
PANI:CNT2	1.5	2.5	1:33
PANI:CNT5	1.5	5.0	1:16
PANI:CNT7	1.5	7.5	1:11
PANI:CNT10	1.5	10.0	1:8
CNT5		5.0	-

Construction of Photovoltaic Devices: the PANI:CNT films were deposited onto patterned PET with evaporated gold. We used gold, but any metal resistant to polyaniline acid could be used. After secondary doping of the films on PET, 70 nm of PEDOT:PSS (with 5% DMSO) was deposited by spin-coating at 6000 rpm. The films were left at 110 °C (in vacuum) overnight to remove water residues and meta-cresol vapors. F8T2 dissolved in chloroform (5 mg mL^{-1}) was then spin-coated at 3000 rpm to obtain a 30-nm-thick layer. The films were then annealed at 100 °C in vacuum for 30 min. Subsequently, 30 nm of C_{60} and 70 nm of Al were thermally evaporated through a mask at a pressure below 10^{-5} mbar.

Characterization: A Shimadzu UV-2450 spectrophotometer was used to obtain absorption spectra of the films deposited onto quartz substrates. Four-point measurements were performed in a Jandel Universal Probe with probes of radius 300 μm separated by 1 mm. The scanning electron microscopy (SEM) images were obtained directly from the films on glass substrates using a Jeol JSM 6360 LV. A thin layer of gold was deposited by sputtering the films prior to measuring. Topographic images of the films on silicon were obtained using a Shimadzu SPM 9500J3 AFM in dynamic mode. The thicknesses of the films were determined using a Dektak 3 profilometer. The reported thickness is an average value of ten measurements. Photovoltaic measurements were performed in a Keithley picoamperimeter (model 6487) with power supply. The solar simulation was performed by an AM 1.5 (air-mass) filter with power illumination of 100 mW cm^{-2} from a 150 W Oriel xenon lamp. Contact angle measurements were performed in a tensiometer Dataphysics, model OCA 15+.

Supporting Information

Supporting Information is available from the Wiley Online Library or from the author.

Acknowledgements

The authors acknowledge the financial support by CNPq, CAPES, NENNAM (PRONEX, Fund. Araucária/CNPq), National Institute of Science and Technology of Carbon Nanomaterials. R.V.S. thanks CAPES for a research fellowship.

Received: July 6, 2012
Revised: September 21, 2012
Published online: October 19, 2012

[1] D. S. Hecht, L. Hu, G. Irvin, *Adv. Mater.* **2011**, *23*, 1482.
[2] D. R. Cairns, R. P. Witte, D. K. Sparacin, S. M. Sachsman, D. C. Paine, G. P. Crawford, R. R. Newton, *Appl. Phys. Lett.* **2000**, *76*, 1425.
[3] S. De, T. M. Higgins, P. E. Lyons, E. M. Doherty, P. N. Nirmalraj, W. J. Blau, J. J. Boland, J. N. Coleman, *ACS Nano* **2009**, *3*, 1767.
[4] J. Zou, H.-L. Yip, S. K. Hau, A. K.-Y. Jen, *Appl. Phys. Lett.* **2010**, *96*, 203301.
[5] S. De, P. E. Lyons, S. Sorel, E. M. Doherty, P. J. King, W. J. Blau, P. N. Nirmalraj, J. J. Boland, V. Scardaci, J. Joimel, J. N. Coleman, *ACS Nano* **2009**, *3*, 714.
[6] A. Kumar, C. Zhou, *ACS Nano* **2010**, *4*, 11.
[7] S.-I. Na, S.-S. Kim, J. Jo, D.-Y. Kim, *Adv. Mater.* **2008**, *20*, 4061.
[8] H. Bejbouji, L. Vignau, J. L. Miane, M.-T. Dang, E. M. Oualim, M. Harmouchi, A. Mouhsen, *Sol. Energy Mater. Sol. Cells* **2010**, *94*, 176.
[9] J. L. Bredas, G. B. Street, *Acc. Chem. Res.* **1985**, *18*, 309.
[10] S. H. Lee, D. H. Lee, K. Lee, C. W. Lee, *Adv. Funct. Mater.* **2005**, *15*, 1495.
[11] D. M. Tigelaar, W. Lee, K. A. Bates, A. Saprigin, V. N. Prigodin, X. Cao, L. A. Nafie, M. S. Platz, A. J. Epstein, *Chem. Mater.* **2002**, *14*, 1430.
[12] Y. H. Kim, C. Sachse, M. L. Machala, C. May, L. Müller-Meskamp, K. Leo, *Adv. Funct. Mater.* **2011**, *21*, 1076.
[13] B. Riedel, I. Kaiser, J. Hauss, U. Lemmer, M. Gerken, *Opt. Express* **2010**, *18*, A631.
[14] J. Jang, J. Ha, K. Kim, *Thin Solid Films* **2008**, *516*, 3152.
[15] B. H. Lee, S. H. Park, H. Back, K. Lee, *Adv. Funct. Mater.* **2011**, *21*, 487.
[16] F. M. Blighe, D. Diamond, J. N. Coleman, E. Lahiff, *Carbon* **2012**, *50*, 1447.
[17] Q. Yao, L. Chen, W. Zhang, S. Liufu, X. Chen, *ACS Nano* **2010**, *4*, 2445.
[18] J. Li, J. Liu, C. Gao, G. Chen, *Int. J. Photoenergy* **2011**, 392832.
[19] C. D. Canestraro, M. C. Schnitzler, A. J. G. Zarbin, M. G. E. da Luz, L. S. Roman, *Appl. Surf. Sci.* **2006**, *252*, 5575.
[20] S. Kim, J. Yim, X. Wang, D. D. C. Bradley, S. Lee, J. C. Mello, *Adv. Funct. Mater.* **2010**, *20*, 2310.
[21] Y. Ma, W. Cheung, D. Wei, A. Bogozi, P. L. Chiu, L. Wang, F. Pontoriero, R. Mendelsohn, H. He, *ACS Nano* **2008**, *2*, 1197.
[22] R. V. Salvatierra, M. M. Oliveira, A. J. G. Zarbin, *Chem. Mater.* **2010**, *22*, 5222.
[23] S. H. Domingues, R. V. Salvatierra, M. M. Oliveira, A. J. G. Zarbin, *Chem. Commun.* **2011**, *47*, 2592.
[24] C. E. Cava, R. V. Salvatierra, D. C. B. Alves, A. S. Ferlauto, A. J. G. Zarbin, L. S. Roman, *Carbon* **2012**, *50*, 1953.
[25] R. Aveyard, *Soft Matter* **2012**, *8*, 5233.
[26] V. B. Menon, A. D. Nikolov, D. T. Wasan, *J. Colloid Interface Sci.* **1987**, *124*, 317.
[27] Z. Jiang, P. Hornsby, R. McCool, A. Murphy, *J. Appl. Polym. Sci.* **2012**, *123*, 2676.
[28] X. Zhang, W. J. Goux, S. K. Manohar, *J. Am. Chem. Soc.* **2004**, *126*, 4502.
[29] R. V. Salvatierra, L. G. Moura, M. M. Oliveira, M. A. Pimenta, A. J. G. Zarbin, *J. Raman Spectrosc.* **2012**, *43*, 1094.
[30] J. Y. Shimano, A. G. MacDiarmid, *Synth. Met.* **2001**, *123*, 251.
[31] W. S. Huang, A. G. MacDiarmid, *Polymer* **1993**, *34*, 1833.
[32] H. Ago, T. Kugler, F. Cacialli, W. R. Salaneck, M. S. P. Shaffer, A. H. Windle, R. H. Friend, *J. Phys. Chem. B* **1999**, *103*, 8116.
[33] M. A. Rodrigues, M.-A. de Paoli, *Synth. Met.* **1991**, *43*, 2957.
[34] A. G. MacDiarmid, A. J. Epstein, *Synth. Met.* **1995**, *69*, 85.
[35] K. Lee, S. Cho, S. Heum Park, A. J. Heeger, C.-W. Lee, S.-H. Lee, *Nature* **2006**, *441*, 65.
[36] L. Bokobza, M. Kolodziej, *Polym. Int.* **2006**, *55*, 1090.
[37] C. F. Matos, F. Galembeck, A. J. G. Zarbin, *Carbon* **2012**, DOI: 10.1016/j.carbon.2012.05.060.
[38] P. N. Adams, P. Laughlin, A. P. Monkman, N. Bernhoeft, *Solid State Commun.* **1994**, *91*, 895.
[39] D. J. Lipomi, J. A. Lee, M. Vosgueritchian, B. C. K. Tee, J. A. Bolander, Z. Bao, *Chem. Mater.* **2011**, *24*, 373.

[40] N. A. D. Yamamoto, A. G. Macedo, L. S. Roman, *J. Nanotechnol.* **2012**, DOI.10.1155/2012/513457.
[41] T. P. Tyler, R. E. Brock, H. J. Karmel, T. J. Marks, M. C. Hersam, *Adv. Energy Mater.* **2011**, *1*, 785.
[42] Y. Zhou, F. Zhang, K. Tvingstedt, S. Barrau, F. Li, W. Tian, O. Inganas, *Appl. Phys. Lett.* **2008**, *92*, 233308.
[43] R. Po, C. Carbonera, A. Bernardi, F. Tinti, N. Camaioni, *Sol. Energy Mater. Sol. Cells* **2012**, *100*, 97.
[44] M. W. Rowell, M. A. Topinka, M. D. McGehee, H.-J. Prall, G. Dennler, N. S. Sariciftci, L. Hu, G. Gruner, *Appl. Phys. Lett.* **2006**, *88*, 233506.
[45] C.-K. Cho, W.-J. Hwang, K. Eun, S.-H. Choa, S.-I. Na, H.-K. Kim, *Sol. Energy Mater. Sol. Cells* **2011**, *95*, 3269.
[46] T. M. Barnes, J. D. Bergeson, R. C. Tenent, B. A. Larsen, G. Teeter, K. M. Jones, J. L. Blackburn, J. van de Lagemaat, *Appl. Phys. Lett.* **2010**, *96*, 243309.
[47] D. Chen, F. Liu, C. Wang, A. Nakahara, T. P. Russell, *Nano Lett.* **2011**, *11*, 2071.
[48] D. Kekuda, J.-H. Huang, K.-C. Ho, C.-W. Chu, *J. Phys. Chem. C* **2010**, *114*, 2764.
[49] M. C. Schnitzler, M. M. Oliveira, D. Ugarte, A. J. G. Zarbin, *Chem. Phys. Lett.* **2003**, *381*, 541.